

# Dielectric liquid microlens with well-shaped electrode

Su Xu, Yeong-Jyh Lin, and Shin-Tson Wu\*

College of Optics and Photonics, University of Central Florida, Orlando, Florida 32816, USA

\*[swu@mail.ucf.edu](mailto:swu@mail.ucf.edu)

**Abstract:** A dielectric liquid microlens with a well-shaped electrode is demonstrated. The bottom well-shaped electrode and the top planar electrode induce an inhomogeneous electric field when a voltage is applied, which causes the focal length to change. Adaptive microlenses and microlens arrays with well-shaped electrode are fabricated and their performance is evaluated. The bi-convex structure introduces a larger optical power. Compared with common planar-electrodes liquid lenses, this well-shaped electrode not only inhibits drifting of the liquid but also reduces the operating voltage.

©2009 Optical Society of America

**OCIS codes:** (0101.1080) adaptive optics; (220.3630) lens; (230.2090) electro-optical devices.

---

## References and links

1. T. Nose, and S. Sato, "A liquid crystal microlens obtained with a non-uniform electric field," *Liq. Cryst.* **5**(5), 1425–1433 (1989).
2. H. Ren, Y. H. Fan, and S. T. Wu, "Tunable Fresnel lens using nanoscale polymer-dispersed liquid crystals," *Appl. Phys. Lett.* **83**(8), 1515–1517 (2003).
3. H. Ren, D. Fox, B. Wu, and S. T. Wu, "Liquid crystal lens with large focal length tunability and low operating voltage," *Opt. Express* **15**(18), 11328–11335 (2007).
4. N. Chronis, G. L. Liu, K. H. Jeong, and L. P. Lee, "Tunable liquid-filled microlens array integrated with microfluidic network," *Opt. Express* **11**(19), 2370–2378 (2003).
5. K. H. Jeong, G. L. Liu, N. Chronis, and L. P. Lee, "Tunable microdoublet lens array," *Opt. Express* **12**(11), 2494–2500 (2004).
6. J. Chen, W. Wang, J. Fang, and K. Varahramyan, "Variable-focusing microlens with microfluidic chip," *J. Micromech. Microeng.* **14**(5), 675–680 (2004).
7. H. Ren, D. Fox, P. A. Anderson, B. Wu, and S. T. Wu, "Tunable-focus liquid lens controlled using a servo motor," *Opt. Express* **14**(18), 8031–8036 (2006).
8. H. Ren, and S. T. Wu, "Variable-focus liquid lens," *Opt. Express* **15**(10), 5931–5936 (2007).
9. L. Dong, A. K. Agarwal, D. J. Beebe, and H. Jiang, "Adaptive liquid microlenses activated by stimuli-responsive hydrogels," *Nature* **442**(7102), 551–554 (2006).
10. S. Grilli, L. Miccio, V. Vespini, A. Finizio, S. De Nicola, and P. Ferraro, "Liquid micro-lens array activated by selective electrowetting on lithium niobate substrates," *Opt. Express* **16**(11), 8084–8093 (2008).
11. L. Miccio, A. Finizio, S. Grilli, V. Vespini, M. Paturzo, S. De Nicola, and P. Ferraro, "Tunable liquid microlens arrays in electrode-less configuration and their accurate characterization by interference microscopy," *Opt. Express* **17**(4), 2487–2499 (2009).
12. M. Vallet, B. Berge, and L. Volvelle, "Electrowetting of water and aqueous solutions on poly (ethylene terephthalate) insulating films," *Polymer (Guildf.)* **37**(12), 2465–2470 (1996).
13. C. C. Cheng, and J. A. Yeh, "Dielectrically actuated liquid lens," *Opt. Express* **15**(12), 7140–7145 (2007).
14. H. Ren, and S. T. Wu, "Tunable-focus liquid microlens array using dielectrophoretic effect," *Opt. Express* **16**(4), 2646–2652 (2008).
15. H. Ren, H. Xianyu, S. Xu, and S. T. Wu, "Adaptive dielectric liquid lens," *Opt. Express* **16**(19), 14954–14960 (2008).
16. S. S. Sridharamurthy, L. Dong, and H. Jiang, "Microfluidic chemical/biological sensing system based on membrane-dissolution and optical absorption," *Meas. Sci. Technol.* **18**(1), 201–207 (2007).
17. S. Reza, and N. A. Riza, "A liquid lens-based broadband variable fiber optical attenuator," *Opt. Commun.* **282**(7), 1298–1303 (2009).
18. H. A. Haus, and J. R. Melcher, "Electromagnetic fields and energy," Chap. 11, [http://web.mit.edu/6.013\\_book/www/chapter11/11.9.html](http://web.mit.edu/6.013_book/www/chapter11/11.9.html)

## 1. Introduction

Two kinds of tunable-focus lenses have attracted much research attention: liquid crystal (LC) lenses [1–3] and liquid lenses [4–15]. Adaptive LC lenses are based on the phase change of the LC medium while adaptive liquid lenses are based on physical adjustment of the lens shape. Compared to an LC lens, the adaptive liquid lens exhibits some attractive features, such as polarization independence, large aperture size, and stronger focusing power. According to the difference in operation principles, adaptive liquid lenses can be further divided into four types: fluidic pressure [4–8], thermal effect [9–11], electro-wetting [12], and dielectrophoresis [13–15]; the latter two have potential applications in cell phone cameras, imaging processing, optical communication, and sensors [12–17]. In an electro-wetting lens, the contact angle on the chamber surface formed by the non-conductive liquid is electrostatically controllable. Thus, the focal length is tunable [12].

In a dielectric lens, under an inhomogeneous electric field, the generated dielectric force causes low dielectric constant liquid to shrink towards the region having a weaker electric field. Due to the interface deformation between these two immiscible dielectric liquids, the focal length becomes tunable. Electrolysis, Joule heating, and microbubble formation often occur in electro-wetting lenses due to the transportation of the free electric charges and the alternating electric fields [12]. Although dielectric lenses do not introduce these problems, they need a patterned-electrode to generate an inhomogeneous electric field, which adds complexity to the fabrication process [12–14]. A non-mechanical method to form uniform liquid droplet arrays was demonstrated, but the droplets could drift in the lens cell, which degrades the lens' stability [14]. Such a problem also exists in dielectric lens with continuous electrodes [15]. Furthermore, they both need a polymer layer to lubricate the substrate surface and enhance the contact angle of the droplet, which introduces electric field shielding effects and increases the driving voltage. For a dielectric lens with a 230  $\mu\text{m}$  aperture and 110  $\mu\text{m}$  cell gap (two liquids with  $\epsilon_1 \sim 47$  and  $\epsilon_2 \sim 5$ ), the focal length changes from  $\sim 620 \mu\text{m}$  to  $\sim 500 \mu\text{m}$  when the driving voltage increases from 0 to 90  $V_{\text{rms}}$ . The optical zoom ratio is  $\sim 1.24$  [15].

In this paper, we demonstrate a tunable dielectric microlens with a top planar electrode and a bottom well-shaped electrode. A glass based plano-convex microlens array stamper is used to form a well-shaped polymer base. After coating a conductive layer onto the base, a well-shaped electrode is achieved, which plays an important role in fixing the position of the microlens and reducing the driving voltage. Furthermore, the polymer layer is not necessarily required, which simplifies the fabrication process and minimizes the electric field shielding effects. Compared to our previous dielectric lens [15], a 1.8X optical zoom is achieved under the same maximum driving voltage while the aperture and cell gap of this new dielectric lens is about 3X larger. We also demonstrate a  $3 \times 3$  microlens array and evaluate its performance. Using different plano-convex microlens array stampers, a microlens array with variable aperture and density can be easily fabricated.

## 2. Device structure and theoretical analysis

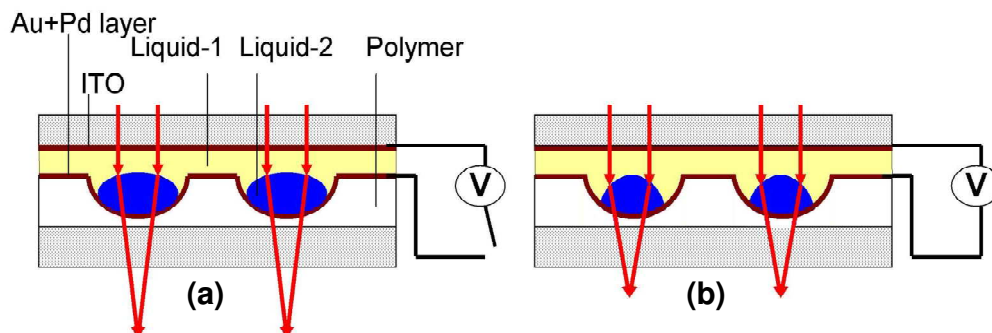


Fig. 1. Side-view structure of the lens cell: (a) Voltage off, and (b) Voltage on.

Figure 1 shows the side-view structure of the microlens cell with well-shaped electrode. From top to bottom, it consists of a planar glass substrate with indium tin oxide (ITO) electrode, liquid-1, liquid-2, a well-shaped polymer base (NOA81) with gold and palladium electrode and a planar glass substrate. Liquid-2 (SantoLight Optical Fluids SL-5267, from Santovac® Fluids) with a low dielectric constant forms a bi-convex droplet on the well-shaped polymer base, while liquid-1 (Glycerol) with a high dielectric constant fills the surrounding space. We choose these two immiscible liquids with similar density in order to minimize the gravity effect. The properties of the two liquids and the polymer well are listed in Table 1.

**Table 1. Properties of liquid-1, liquid-2, and polymer well.**

	Dielectric Constant	Refractive Index	Density (g/cm <sup>3</sup> )	Color
Liquid-1	42	1.47	1.26	Clear
Liquid-2	4.7	1.67	1.25	Clear
Polymer Well	4.0	1.56	1.2	Clear

In the relaxed state, the curvature of the droplet is minimal. In a voltage-on state, the bi-convex liquid droplet will induce an inhomogeneous electric field. According to Kelvin theory, the dielectric force exerted on the droplet can be expressed as [18]

$$\vec{F} = \frac{\epsilon_0}{2} (\epsilon_1 - \epsilon_2) \nabla (E \cdot E), \quad (1)$$

where  $\epsilon_0$ ,  $\epsilon_1$  and  $\epsilon_2$  donate the permittivity of free space, liquid-1, and liquid-2, respectively, and  $E$  denotes the electric field on the curved droplet surface. From Eq. (1), the difference between  $\epsilon_1$  and  $\epsilon_2$  and the gradient of the electric field play key roles on the dielectric force. When the dielectric force is strong enough, liquid-1 and liquid-2 will move toward the region with strong and weak electric fields, respectively. The droplet tends to contract and the surface profile of the droplet is reshaped. As a result, the focal length becomes shorter, as shown in Fig. 1(b).

According to Eq. (1), the dielectric force originates from the inhomogeneous electric field. In a common planar-electrode structure, the dielectric force is induced only from the shape of the droplet. Thus, the cell gap should be larger than the apex distance of the droplet in order to leave some space for the droplet to contract [15]. By contrast, our well-shaped electrode structure introduces non-uniform electric fields from both the non-planar electrode and the bi-convex shape of the droplet, resulting in an enhanced electric field gradient. The gap between the two electrodes is also reduced because the bottom electrode is deposited on the well surface and not on the glass substrate. With the enhanced non-uniform electric field and the closer electrode gap, the dielectric force is increased and the driving voltage is reduced.

We also conducted simulations to investigate and compare the dielectrophoresis in these two structures with an operating voltage of 100 V<sub>rms</sub>, and the results are shown in Fig. 2. The colors in the figure represent the electric field strength corresponding to the bottom color bar. According to Eq. (1), a larger electric field gradient induces a larger dielectric force. In a common planar-electrode structure shown in Fig. 2(a), both liquids experience a similar electric field as indicated by the dark blue color. The electric field gradient could only be found along the interface between two liquids near the bottom planar electrode, which only represents ~1/4 of the arc of droplet. The white arrows denote the dielectric force acting on the droplet. However, in a well-shaped electrode structure shown in Fig. 2(b), the color difference along the entire interface between the two liquids indicates that an electric field gradient exists in more than 1/3 of the arc. A much larger surface is thus affected by the dielectrophoresis, and the generated electric force is indicated by the orange arrows in Fig. 2(b). The downward force acting at the apex of the droplet would weaken the droplet deformation and focus change, but it is relatively small. Because of the stronger electric fields originating from the closer electrode gap, and the larger affected surface, the operating voltage

of the lens with well-shaped electrode will be lower than that of the lens with common planar-electrodes having the same aperture and cell gap dimensions.

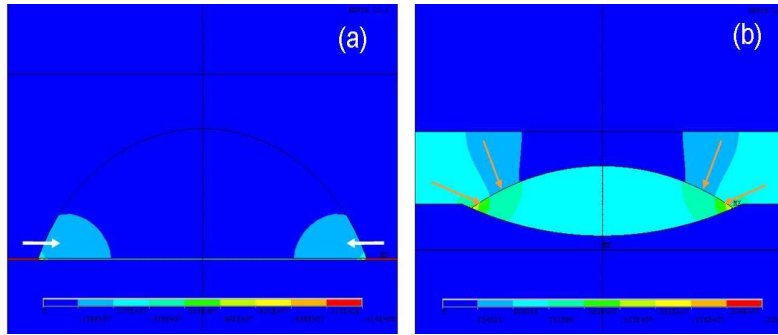


Fig. 2. Simulation results of the electric field of the two structures at  $V = 100V_{\text{rms}}$  (a) common planar-electrodes, and (b) top planar-electrode and bottom well-shaped electrode.

### 3. Experiment

Figure 3 shows the device fabrication procedure. Four steps are involved. In Fig. 3(a), we injected adhesive into a glass cell. The cell was composed of a bottom glass substrate and a glass-based plano-convex microlens array ( $R = 1 \text{ mm}$ ,  $\text{Ø} = 0.75 \text{ mm}$ ,  $6 \times 6$ , from ISUZU GLASS), which was used as a stamper. After UV exposure, the stamper was peeled off and the solidified concave microlens pattern was left on the bottom glass substrate, as depicted in Fig. 3(b). In Fig. 3(c), a conducting layer consisting of a mixture of gold and palladium was deposited on the concave microlens as the bottom electrode using a sputter coater (from EMITECH). Finally, after dropping liquid-2 and liquid-1, a planar glass with ITO was used as top substrate to seal the cell, as Fig. 3(d) shows. The cell gap is  $\sim 270 \mu\text{m}$ . The total transmission of the lens is  $\sim 50\%$  at  $\lambda = 550 \text{ nm}$ . Most of this loss originates from absorption of the metal electrode and from interface reflections. This can be improved by optimizing the materials and thickness of the bottom electrode and by depositing substrates with anti-reflection coatings.

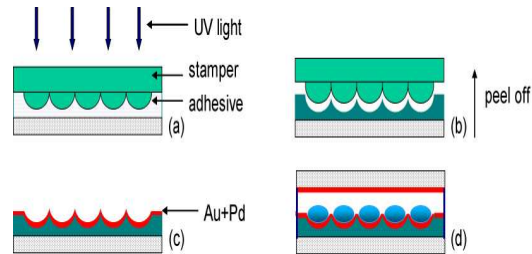


Fig. 3. Side view of the device fabrication procedure: (a) Making lens cell and UV exposure, (b) Peeling off the stamper, (c) Coating Au + Pd electrode, and (d) Dropping liquids and sealing the cell.

### 4. Results and discussion

It is convenient to evaluate the microlens performance using an optical microscope. The lens encapsulated in the cell was placed on a microscope stage which can move along the vertical direction. First, we observed the two-dimensional (2D) focus spot of a liquid droplet (diameter  $\sim 700 \mu\text{m}$ ). At  $V = 0$ , we focused on the droplet's surface and the image is shown in Fig. 4(a). The droplet is quite circular and has a clear border with the surrounding liquid. We then adjusted the position of the lens cell to get the minimum focus spot, as shown in Fig. 4 (b). An image of the number "3" was captured as shown in Fig. 4(c). The light is highly centrally focused, the image is clear, and there is no obvious noise that occurs in the dark background,

which implies the microlens has as good focusing ability as that of a conventional solid lens. Minor scattering is observed, though, due to slight nonuniformity of the well-shaped electrode, which is induced by the relatively slow stage rotation speed of the sputter coater. The optic axis of the liquid lens could be slightly deviated from its normal because of the nonuniform surface of the bottom well-shaped electrode, which induces a non-spherical profile in a voltage-on state. The resolution of the dielectric lens was also measured through the microscope. Figure 4(d) shows the image of a 1951 U.S. Air Force (USAF) resolution target taken in the transmission mode by the microscope. The highest resolution of the device is  $\sim 181$  lp/mm as the patterns of group 7 number 4 are still resolvable. To visually observe the tunable state with different operating voltages, a movie for tuning the above microlens was taken, as shown in Fig. 4(e). A small number “2” on the USAF resolution target was used as an object and placed under the lens cell. At  $V = 0$ , the droplet was in a defocused state and the image was very blurry. When the lens was actuated at  $40V_{\text{rms}}$  a small inverted image “2” began to appear. The image kept zooming in as we gradually increased the driving voltage to  $V_{\text{max}} = 88V_{\text{rms}}$ . Fixing the position of the cell, we observed only one clearest imaging state during this continuous voltage scan. This indicates that the focal length of the droplet is electrically tunable.

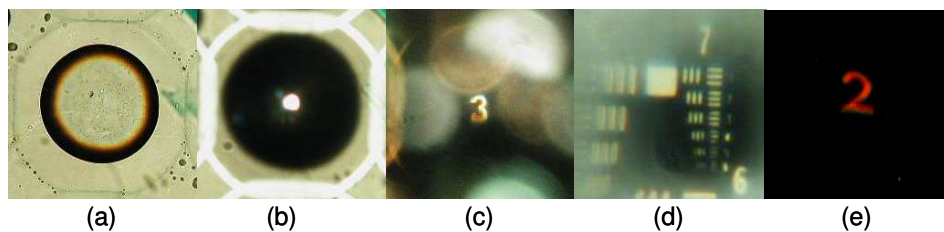


Fig. 4. (a) The image of the lens cell at the position of surface focus, (b) At the position of the smallest spot size, (c) Image at focus, (d) Resolution test, and (e) Tunable state of the lens driven from 0 to  $88V_{\text{rms}}$  (Media 1).

The focal length of the dielectric lens shown in Fig. 4(a) was measured at different voltages through the same microscope. The voltage dependent focal length is plotted in Fig. 5(a) as blue dots. At  $V = 0$ , the inherent focal length of the microlens is  $\sim 2.50$  mm. As the voltage increases, the focal length gradually decreases. At  $V = 88 V_{\text{rms}}$ , it is decreased to  $\sim 1.39$  mm. Compared to the previous dielectric lens [15], the present dielectric lens with well-shaped electrode achieves a 1.8X optical zoom under the same voltage, with a  $\sim 3X$  larger aperture and cell gap. The operating voltage can be dramatically reduced if the aperture and cell gap of the lens become smaller. Because the diameter of each droplet is small and its shape is nearly spherical, we use ZEMAX to calculate the theoretical focal length. Only the well-shaped polymer base, liquid-1 and liquid-2 are considered. The lens structure and parameters used for the ZEMAX simulation are shown in Fig. 5(b), where  $n_1$ ,  $n_2$ , and  $n_p$  donate the refractive index of liquid-1, liquid-2, and well-shaped polymer base, respectively,  $D$  is the initial diameter of the lens,  $d$  is the cell gap of lens cell, and  $t_p$  is the apex distance of the polymer base.  $R_1$  is the curvature radius of the well-shaped base, which is equal to that of the plano-convex microlens array stamper, because this base is replicated from the stamper.  $R_2$  is the curvature radius of the top lens surface,  $t$  is the apex distance of the lens. Both  $R_2$  and  $t$  vary with the operating voltage. All of these parameters will affect the dynamic range of the lens. When other parameters are kept constant, the dynamic range varies with  $R_1$ . Therefore, we may specially design  $R_1$  to provide the dynamic range we need. In our experiment,  $R_1 = 1$  mm as purchased. Since the deformation of a liquid droplet profile is related to the balance of electric energy, surface energy, adhesion energy, and gravitational energy [13], a reliable theoretical model should take these factors into consideration in order to depict the droplet profile change and predict the dynamic range of the lens more accurately. In experiment, to achieve a large dynamic range with a low voltage remains a technical challenge.

In the relaxed state, we measured the apex distance  $t \sim 0.163$  mm, so the calculated focal length is  $\sim 2.45$  mm, which is in good agreement with the measured focal length (2.50 mm). Meanwhile, the largest apex distance  $t$  is  $\sim 0.237$  mm since the measured  $t_p \sim 0.032$  mm and  $d \sim 0.270$  mm. The sum of  $t$  and  $t_p$  should be smaller than  $d$ . Otherwise, the droplet will touch the top glass substrate. The calculated focal length at this limiting state is  $\sim 1.25$  mm, which is slightly shorter than the measured data ( $\sim 1.39$  mm) at  $V = 88$  V<sub>rms</sub>. This small difference could result from the fact that the microlens is not driven to its limiting state in our experiment.

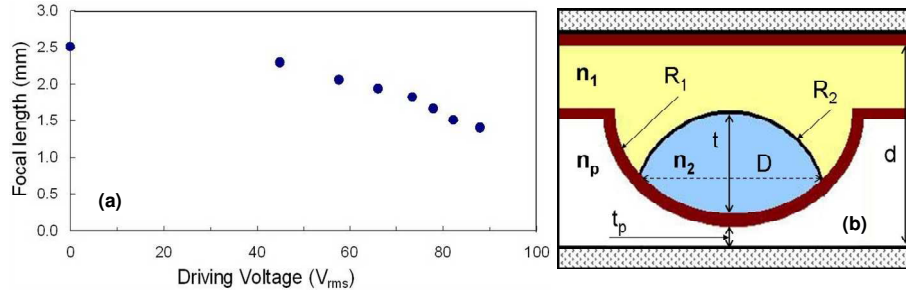


Fig. 5. (a) Measured focal length of the microlens at different driving voltages, and (b) Lens structure and parameters for ZEMAX simulation.

We also demonstrated a  $3 \times 3$  microlens array and evaluated its performance. The imaging properties of the microlens array are shown in Fig. 6(a). Due to differences in the shape and diameter of the microlenses in the array, they are slightly different in focal length. As shown in Fig. 6(b), the borders of some spots are red, which implies that those are inside of the focus, while the blue color borders mean outside of the focus. The uniformity of the microlens array will be greatly improved if the liquid droplets are prepared by machine rather than by hand. To visually observe the tunable state according to different voltages, a movie for tuning this  $3 \times 3$  microlens array was taken, shown in Fig. 6(c). The contracting speed of the microlens array is fast, but the relaxing speed is a bit slow ( $\sim 500$  ms) as it depends on the viscosity of the liquids and the related interfacial tensions [15]. The viscosity of the surrounding liquid-1 is  $\sim 1.5$  Pas, introducing a large hysteresis when the voltage is switched off. The relaxing time can be shortened if we use some low viscosity liquids.

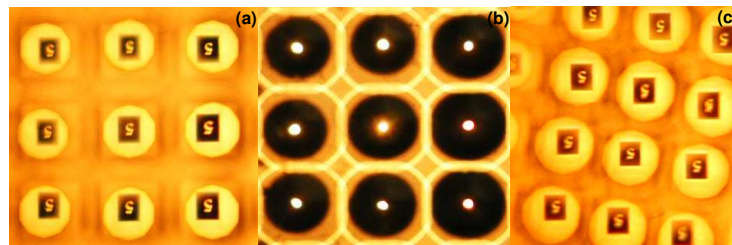


Fig. 6. (a) Imaging properties of the microlens array, (b) Microlens array, and (c) Tunable state of the lens driven between 0V and 88V<sub>rms</sub> (Media 2).

## 5. Conclusion

A tunable dielectric liquid microlens with a well-shaped electrode is demonstrated. The well-shaped electrode structure and the bi-convex shape of the liquid droplet both have the ability to induce an inhomogeneous electric field, which not only fixes the position of the microlens, but also reduces the operating voltage as compared to a microlens with common planar electrodes. A microlens with 1.8X optical zoom under  $V = 88$  V<sub>rms</sub> is achieved. The transmission and scattering of the lens can be improved by coating ITO on the well-shaped polymer base. The response time can be shortened using low-viscosity liquids. Such a liquid

microlens shows potential applications in cell phone cameras, imaging processing, optical communication and beam steering. We also propose the possibility of fabricating microlens arrays with different aperture and density using a simple method.